NONLOCAL EFFECT ON THE PULL-IN INSTABILITY ANALYSIS OF GRAPHENE SHEET NANOBEAM ACTUATOR

M. X. Lin

Department of Mechanical Engineering
National Cheng-Kung University
Tainan, Taiwan

S. Y. Lee

Department of Mechanical Engineering
National Cheng-Kung University
Tainan, Taiwan

C. K. Chen

Department of Mechanical Engineering
National Cheng-Kung University
Tainan, Taiwan

ABSTRACT

In this study, the pull-in phenomenon of a Nano-actuator is investigated employing a nonlocal Bernoulli-Euler beam model with clamped-clamped conditions. The model accounts for viscous damping, residual stresses, the van der Waals (vdW) force and electrostatic forces with nonlocal effects. The hybrid differential transformation/finite difference method (HDTFDM) is used to analyze the nonlocal effects on a graphene sheet nanobeam, which is electrostatically actuated under the influence of the coupling effect, the von Kármán nonlinear strains and the fringing field effect. The pull-in voltage as calculated by the presented model deviates by no more than 0.29% from previous literature, verifying the validity of the HDTFDM. Furthermore, the nonlocal nonlinear behavior of the electrostatically actuated nanobeam is investigated, and the effects of viscous damping, residual stresses, and length-gap ratio are examined in detail. Overall, the results reveal that small scale effects significantly influence the characteristics of the graphene sheet nanobeam actuator.

Keywords: Pull-in voltage, Nonlocal elasticity theory, The hybrid differential transformation/finite difference method, Nanoactuator.

1. INTRODUCTION

In recent years, micro-electro-mechanical systems (MEMS) and nano-electro-mechanical systems (NEMS) have seen a diverse range of applications, including nano-switches, MEMS gyroscopes, radio-frequency (RF) devices, photonic crystals, and biosensors [1-5]. Electrostatic actuators have a lot of advantages such as simple design, rapid response, low power consumption, and effective integration with MEMS and manufacturing techniques. The present work investigates the pull-in phenomena of nano-switches subjected to an electrostatic force from an applied voltage, incorporating the influence of the fringing field effect, the residual stress, and the effect of viscous damping within the nonlocal elasticity theory to account for small scale effects. When voltage is applied across a movable and a stationary conducting electrode, a distributed electrostatic force is created between the electrodes. When the voltage reaches a critical value, the movable electrode becomes unstable, and collapses onto the stationary electrode. The voltage at this critical value is known as the pull-in voltage. This phenomenon is important in the design of MEMS and NEMS.

Researches highlight some problems arising from consideration of micro-scale to nano-scale interactions.

* Corresponding author (ckchen@mail.ncku.edu.tw)

DOI : 10.1017/jmech.2018.41
Copyright © 2019 The Society of Theoretical and Applied Mechanics
https://doi.org/10.1017/jmech.2018.41 Published online by Cambridge University Press

Examples include intermolecular forces to be considered, such as the Casimir force and the van der Waals force [6]. The Casimir is an attractive force between two flat parallel plates of solids resulting from quantum fluctuations. The vdW force representes the electrostatic interaction between pairs of magnetic poles [7]. Nano-scale effects have significant impact on nano-switches. The intermolecular forces influence the accuracy of analysis of the structure, so both the Casimir force and the van der Waals force must be taken into account in the analysis of NEMS [8]. However, when the gap between the movable electrode and stationary electrode is below 20 nm, the vdW force between two electrodes is dominate, and it suffices to consider only the van der Waals force. But when the gap between the movable electrode and stationary electrode is above 20 nm and less than several tens of micrometers, the Casimir force must be teken into account [7, 9]. Mousavi *et al*. [10] used the nonlocal Euler–Bernoulli beam model to study the small scale effects on the pull-in instability of nano-switches subjected to electrostatic forces and intermolecular forces by using the differential quadrature method. Dequesnes *et al*. [11] investigated the significance of vdW force on the pull-in voltage characteristics of carbon-nanotube-based NEMS in the design of NEMS switches based on a lumped model to compute the pull-in voltage of cantilever and fixed–fixed switches. Ramezani *et al*. [12] transformed nonlinear differential equations into the integral form by using the Green's function of the cantilever beam, and the results showed that the influence of the van der Waals force on pull-in voltage and deflection of cantilever type NEMS switches was significant. Lin and Zhao [13] used a one-degree-of-freedom mass-spring model to investigate the influence of the Casimir force on the nonlinear behavior of a nanoscale electrostatic actuator.

In recent years, graphene has been widely investigated because of its remarkable mechanical properties, thermal diffusivity, strength, and electrical conductivity. Graphene is a single layer of graphite crystal, one carbon atom thick. Single-layered graphene sheets consist of carbon atoms which are covalently bonded in a honeycomb lattice. Pradhan and Murmu [14] used nonlocal continuum theories to account for the small size effects on the buckling of single-layered graphene sheets under biaxial compression by using the differential quadrature method. The results show that the nonlocal effect is significant in graphene sheets and has a decreasing effect on buckling loads. Murmu and Pradhan [15] investigated the stability response of single-walled carbon nanotubes (SWCNTs) embedded in an elastic medium, using nonlocal elasticity, Timoshenko beam theory and the differential quadrature method. Both Winkler-type and Pasternak-type foundation models are taken into consideration. Numerical results show that SWCNT are strongly dependent on nonlocal small-scale coefficients and the stiffness of the surrounding medium.

In the past, the research on the microactuator had been proposed based on the classical continuum theory. When the scale of the structure become small, classical continuum theory is not exact enough to analyze the nanoactuator because it ignores size-dependent effects, which experiments and molecular dynamic simulations have shown to significantly influence mechanical properties. To solve this problem, various size-dependence continuum theories, such as the modified couple stress theory, nonlocal elasticity theory, and the strain gradient theory have been applied in research. The most used continuum theory for analyzing the nano-scale research is nonlocal elasticity theory [16-19], which has been applied to nano-scale problems by several researchers. Murmu and Pradhan [20] implemented nonlocal elasticity theory to analyze nano-single-layered graphene sheets embedded on an elastic foundation. The numerical results showed that the fundamental frequencies of a single-layered-graphene sheet are strongly dependent on small-scale coefficients. Yang *et al*. [21] used nonlocal elasticity theory to investigate the pull-in behavior of nano-switches subjected to an electrostatic force from an applied voltage, incorporating intermolecular forces with nonlocal elasticity theory to account for small scale effects. Cantilever nano-beams and fixed–fixed nano-beams are taken into account in the nano-switches by linear distributed load model. The effects of gap ratio and slenderness ratio on the nano-switches are discussed in detail. Reddy [22] derived results based on various beam theories – Euler-Bernoulli, Timoshenko, Reddy, and Levinson – using the nonlocal constitutive relation of the nonlocal elasticity theory and von Kármán nonlinear strains and produced exact solutions of deflection and natural frequencies. Najar *et al*. [23] investigated small scale effects on the nonlinear static and dynamic response subjected to a DC voltage. The nanoactuator was modeled as an Euler–Bernoulli beam and it is simulated with both cantilever and fixed-fixed boundaries. Numerical results show that the maximum stable deflection applied to DC voltage is influenced by small scale effect and the dynamic response is also investigated by small scale effect on the natural frequencies.

The nonlinear behaviors of a graphene nanobeam can be treated using the differential transformation theory, which transforms the governing equation into an algebraic equation through Taylor's series expansion. Zhou [24] first applied this method to solve the linear and nonlinear phenomena problems in electric circuit problems. Yu and Chen [25] combined the differential transformation method and finite difference scheme to obtain a numerical solution to the Blasius equations, demonstrating the differential transformation method as a powerful method for nonlinear problems. Chen *et al*. [26] investigated the entropy generation within a mixed convection flow with viscous dissipation effects in a parallel-plate vertical channel with the differential transformation method. The calculated velocity and temperature fields are in good agreement with the analytical solutions. Chen *et al*. [27] combined the hybrid differential transformation and finite difference method to analyze the dynamic response of an electrostatically actuated micro fixed-fixed beam. The analysis of their research focused on the correlation between beam deflection and the magnitude of the applied voltage.

It should be noted that the Euler–Bernoulli beam neglects the effects of shear deformation and rotatory inertia, which are considered in Timoshenko beam theory. The

https://doi.org/10.1017/jmech.2018.41 Published online by Cambridge University Press

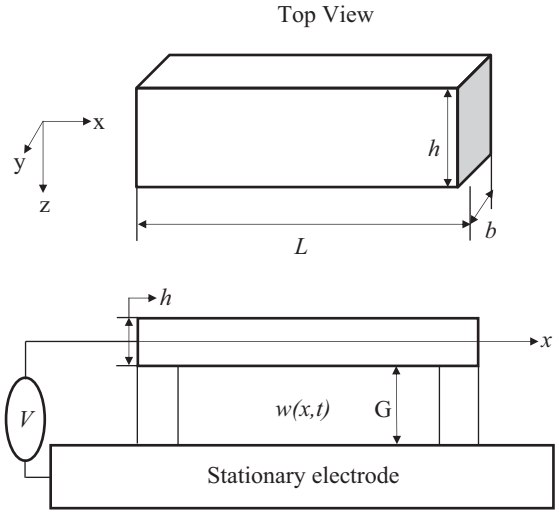


Fig. 1 Illustration of the actuated clamped-clamped nanobeam.

graphene sheet considered in the present study can be modelled as a slender beam; Euler-Bernoulli beam theory is therefore applicable in the investigation of its pull-in behavior. The model is solved with clamped-clamped boundaries and under DC actuating conditions and takes account of the viscous damping, residual stresses, and vdW force with nonlocal effects. In this study, a technique combining both the differential transformation and the finite difference method is developed to discretize the time and space domains of the graphene sheet nanobeam. The validity of the hybrid scheme is confirmed by comparing the results with previous literature. The analysis of this study focuses on the nonlocal effects of viscous damping, residual stresses, and length-gap ratio, and their influences on the pull-in voltage of the graphene sheet nanobeam actuator.

2. MODEL FORMULATION

Figure 1 shows an illustration of the clamped-clamped nanobeam actuator with a nanobeam of length L, width b, and thickness h. The initial gap between the movable electrode, and stationary electrode is denoted by G. The present study considers von Kármán nonlinear strains, the fringing field effect, viscous damping, residual stress and nonlocal effect, which are integrated to form governing equation for the graphene nanobeam which is nonlocal and nonlinear. The nonlinear term in the governing equation is expanded as a Taylor series, and the equations are solved using HDTFDM.

2.1 Nonlocal Elasticity Model

Nonlocal elasticity model is proposed by Eringen [16], which accounts for the scale effect between the size-effect and mechanical properties. The stress at a point is assumed to be dependent on the strain at all the points in the continuum structure. The constitutive equations for a nonlocal elastic structure are expressed as

$$\bar{\sigma}(\mathrm{x}) = \int_v \lambda\left(|\mathrm{x}' - \mathrm{x}|, \tau\right)\sigma(\mathrm{x}')dV(\mathrm{x}') \tag{1}$$

where $\bar{\sigma}$ is the stress tensor at point x. $\lambda(|x' - x|, \tau)$ is the kernel function and represents the nonlocal effects at the point x by the influence of point x' with the distance of $|x' - x|$. τ is a material parameter defined as $e_0 a/\ell$, where e_0 is a constant determined according to experimental results.

The Eq. (1) is difficult to solve. Therefore, Eringen [17] proposed a simplified constitutive model

$$\left(1 - \mu_0 \nabla^2\right)\bar{\sigma} = \sigma, \quad \mu_0 = (e_0 a)^2 = (\tau \ell)^2 \tag{2}$$

where a is an internal characteristic length, ℓ is an external characteristic length, and ∇^2 is the Laplace operator.

2.2 Modeling of Clamped-Clamped Nanobeam

In NEMS, when the gap separation is below 20 nm, only the van der Waals force is considered. The governing equation for the deflection of the clamped-clamped nanobeam has been derived and presented in the research [23]. In analyzing the deflection of the clamped-clamped nanobeam, we consider only the effects of vdW force, first-order fringing field, and von Kármán nonlinear strains on the electrostatic forces, and neglect the initial deflection and the Casimir force. The nonlocal nonlinear governing equation in this model can be written:

$$\tilde{E}I\frac{\partial^4 w}{\partial x^4} - \left(\frac{\tilde{E}A}{L}\int_0^L\left[\frac{1}{2}\left(\frac{\partial w(x,t)}{\partial x}\right)^2\right]dx + N_0\right)\left(1 - (e_0 a)^2\nabla^2\right)\frac{\partial^2 w}{\partial x^2} + \left(1 - (e_0 a)^2\nabla^2\right)\left(\rho h\frac{\partial^2 w}{\partial t^2} + c\frac{\partial w}{\partial t}\right)$$

$$= \left(1 - (e_0 a)^2\nabla^2\right)\left(\frac{\varepsilon b V^2}{2(G-w)^2}\left(1 + 0.65\frac{G-w}{b}\right) + \frac{A_0 b}{6\pi(G-w)^3}\right) \tag{3}$$

where ε_0, A and G are respectively the permittivity of free space, the cross-sectional area of clamped-the clamped nanobeam, and the initial gap distance between two electrodes. V is the applied voltage, and N_0 is the residual stress. $I = bh^3/12$ is the second moment of inertia of the clamped-clamped nanobeam, and E is the Young's modulus of the beam. $\tilde{E}$ is the effective beam material modulus. When $b \geq 5h$, then $\tilde{E}$ becomes the plate modulus $E/1\text{-}\upsilon^2$ based on the previ-

https://doi.org/10.1017/jmech.2018.41 Published online by Cambridge University Press

ous study, where υ is the Poisson's ratio. The deflection w is a function of position x and time t, denoted by $w = w(x, t)$.

Considering the fringing field effect, the electrostatic force per unit length of the beam can be written as [21]

$$F_{elec} = \frac{\varepsilon b V^2}{2(G-w)^2}\left(1+0.65\frac{G-w}{b}\right) \tag{4}$$

where the first order fringing field correction is equal to 0.65. The van der Waals force per unit length of the beam can be expressed as [21]

$$F_{vdW} = \frac{A_0 b}{6\pi(G-w)^3} \tag{5}$$

where A_0 is the Hamaker constant.

The boundary conditions of this model are specified as follows:

$$\begin{aligned} &w(x,t) = \frac{\partial w(x,t)}{\partial x} = 0 \quad \text{at} \quad x = 0 \\ &w(x,t) = \frac{\partial w(x,t)}{\partial x} = 0 \quad \text{at} \quad x = L \end{aligned} \tag{6}$$

The initial condition is given by

$$w(x,0) = \frac{\partial w(x,0)}{\partial t} = 0 \tag{7}$$

2.3 Dimensionless Parameters of the Governing Equation

For convenience of analysis, dimensionless parameters are introduced:

$$\begin{aligned} &w^* = \frac{w}{G}, \quad x^* = \frac{x}{L}, \quad t^* = \frac{t}{T_c}, \quad T_c = \sqrt{\frac{\rho A L^4}{\tilde{E}I}}, \quad c^* = \frac{cL^4}{\tilde{E}IT_c}, \quad N^* = \frac{NL^2}{\tilde{E}I}, \quad \alpha_0 = \left(\frac{e_0 a}{L}\right)^2, \\ &\alpha_1 = \frac{\varepsilon_0 b L^4 V^2}{2\tilde{E}IG^3}, \quad \alpha_2 = 0.65\frac{G}{b}, \quad \alpha_3 = \frac{A_0 b L^4}{6\pi\tilde{E}IG^4}, \quad \alpha_4 = \frac{6G^2}{h^2} \end{aligned} \tag{8}$$

Using the above dimensionless parameters, the governing equation can be expressed as follows:

$$\begin{aligned} &\frac{\partial^4 w^*}{\partial x^{*4}} + \frac{\partial^2 w^*}{\partial t^{*2}} - \alpha_0 \frac{\partial^4 w^*}{\partial x^{*2}\partial t^{*2}} - \left(\alpha_4 \int_0^1 \left(\frac{\partial w^*}{\partial x^*}\right)^2 dx^* + N^*\right)\frac{\partial^2 w^*}{\partial x^{*2}} + c^*\frac{\partial w^*}{\partial t^*} - \alpha_0 c^* \frac{\partial^3 w^*}{\partial x^{*2}\partial t^*} \\ &+ \left(\alpha_0\alpha_4 \int_0^1 \left(\frac{\partial w^*}{\partial x^*}\right)^2 dx^* + N^*\right)\frac{\partial^4 w^*}{\partial x^{*4}} = \frac{\alpha_1}{(1-w^*)^2} - \left(\frac{6\alpha_0\alpha_1}{(1-w^*)^4}\right) + \frac{\alpha_1\alpha_2}{(1-w^*)} - \left(\frac{2\alpha_0\alpha_1\alpha_2}{(1-u^*)^3}\right) + \frac{\alpha_3}{(1-w^*)^3} - \left(\frac{12\alpha_0\alpha_3}{(1-w^*)^5}\right) \end{aligned} \tag{9}$$

The corresponding boundary conditions become

$$\begin{aligned} &w^*(x^*,t^*) = \frac{\partial w^*(x^*,t^*)}{\partial x^*} = 0 \quad \text{at} \quad x^* = 0 \\ &w^*(x^*,t^*) = \frac{\partial w^*(x^*,t^*)}{\partial x^*} = 0 \quad \text{at} \quad x^* = 1 \end{aligned} \tag{10}$$

The initial condition can be represented as

$$w^*(x^*,0) = \frac{\partial w^*(x^*,0)}{\partial t^*} = 0 \tag{11}$$

The nonlinear term in Eq. (9) can be approximated by using Taylor series expansion and ignoring the higher-order terms, and the governing equation can be represented as

https://doi.org/10.1017/jmech.2018.41 Published online by Cambridge University Press

Table 1 Comparison of hybrid results and LDL method results for pull-in voltage.

	HDTFDM	LDL method [21]	Δe (%)
Pull-in voltage(V)	10.29	10.26	0.29

$$\Delta e = \frac{|LDL\ \ method - Hybrid\ \ method|}{LDL\ \ method} \times 100\%$$

Table 2 Free end gaps under various pull-in voltages.

Voltage (V)	Free end gap (um)			
	Finite difference method [28]	Analytical [29]	Experiment [29]	Present work
20	90.334	90.2	90.5	90.2
40	84.827	84.3	84.6	84.11
60	76.516	71.5	70	69.42

Table 3 Material and geometry properties of nanobeam model.

Parameter	Graphene [14, 20]
Young's modulus (E) (TPa)	1
Poisson's Ratio (v)	0.25
Density (ρ) (kg/m^3)	2250
Permittivity of free space (ε_0) (F/m)	8.854×10^{-12}
Width of the beam (b) (nm)	1.8
Thickness of the beam (h) (nm)	0.35
Initial gap (G) (nm)	1.8
Length of the beam (L) (nm)	20

$$\frac{\partial^4 w^*}{\partial x^{*4}} + \frac{\partial^2 w^*}{\partial t^{*2}} - \alpha_0 \frac{\partial^4 w^*}{\partial x^{*2} \partial t^{*2}} - \left(\alpha_4 \int_0^1 \left(\frac{\partial w^*}{\partial x^*} \right)^2 dx^* + N^* \right) \frac{\partial^2 w^*}{\partial x^{*2}} + \left(\alpha_0 \alpha_4 \int_0^1 \left(\frac{\partial w^*}{\partial x^*} \right)^2 dx^* + N^* \right) \frac{\partial^4 w^*}{\partial x^{*4}}$$

$$+ c^* \frac{\partial w^*}{\partial t^*} - \alpha_0 c^* \frac{\partial^3 w^*}{\partial x^{*2} \partial t^*} = \alpha_1 \left(1 + 2w^* + 3w^{*2} + 4w^{*3} + 5w^{*4} + 6w^{*5} \right)$$

$$- 6\alpha_0 \alpha_1 \left(1 + 4w^* + 10w^{*2} + 20w^{*3} + 35w^{*4} + 56w^{*5} \right) + \alpha_1 \alpha_2 \left(1 + w^* + w^{*2} + w^{*3} + w^{*4} + w^{*5} \right)$$

$$- 2\alpha_0 \alpha_1 \alpha_2 \left(1 + 3w^* + 6w^{*2} + 10w^{*3} + 15w^{*4} + 21w^{*5} \right) + \alpha_3 \left(1 + 4w^* + 10w^{*2} + 20w^{*3} + 35w^{*4} + 56w^{*5} \right)$$

$$- 20\alpha_0 \alpha_3 \left(1 + 6w^* + 21w^{*2} + 56w^{*3} + 126w^{*4} + 252w^{*5} \right) \tag{12}$$

In this study, the differential transformation method and finite difference method [26-27] are applied respect to time and space domain in Eq. (12) respectively (see Appendix A).

3. RESULTS AND DISCUSSIONS

The validity of the HDTFDM is verified by comparing the pull-in voltage of clamped-clamped nanobeam with result reported by Yang *et al*. [21] based on the LDL (linear distributed load) method. The parameters used in the numerical example are L = 200 nm, E = 166 Gpa, b = 30 nm, h = 3.5 nm, and G = 30 nm. The Casimir force is used in the numerical example. As shown in Table 1, it is observed that the solutions are in good agreement with the numerical results of two other different methods, with a deviation of no more than 0.29%. Moreover, the results show a good agreement with the numerical and experimental results obtained [28, 29], as shown in Table 2.

Figure 2 shows the results obtained by HDTFDM for the nonlinear behavior of the clamped-clamped nanobeam with the applied voltage values range from 5 V to 10.29 V. The results show that the deflection of the nanobeam is symmetrical about the center point because of the clamped-clamped boundary condition. The deflection of the nano-beam increases as the applied voltage increases because of the electrostatic force driving the conducting electrodes. The nanobeam collapses when the voltage reaches 10.29 V; this critical value is called the pull-in voltage. Figure 3

https://doi.org/10.1017/jmech.2018.41 Published online by Cambridge University Press

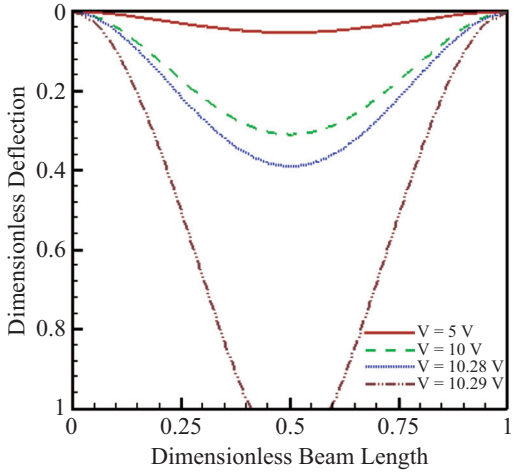


Fig. 2 Deflection of clamped-clamped nanobeam for different voltages.

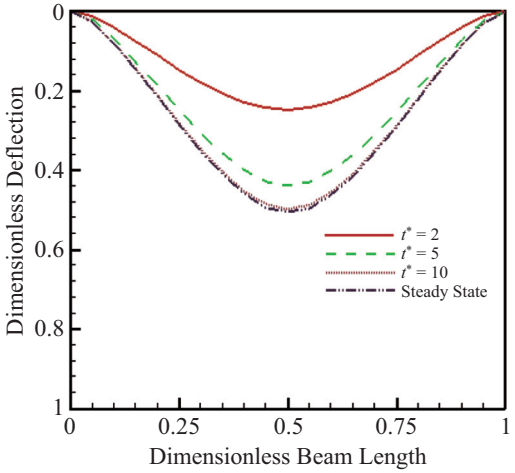


Fig. 3 Dynamic behavior of the clamped-clamped nanobeam for different dimensionless time (Voltage = 10 V).

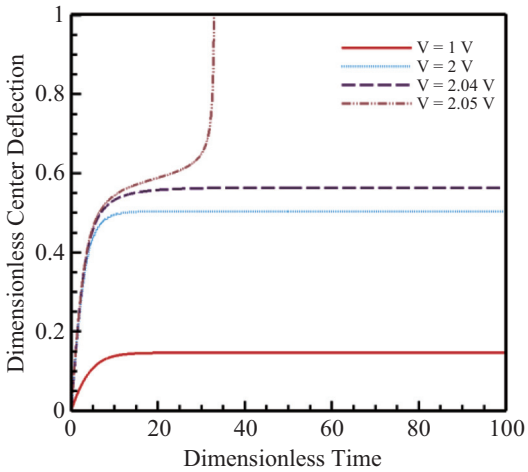


Fig. 4 Variation of dimenisionless center deflection over time as function of DC voltage.

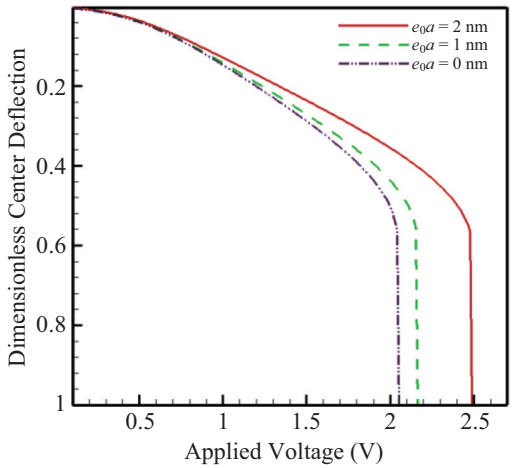


Fig. 5 Variation of dimensionless center deflection with applied voltage for different scale parameters.

illustrates the result obtained by the HDTFDM for the dynamic behavior of the clamped-clamped nanobeam at a voltage of 10 V. It can be observed that the deflection at the center increases with the dimensionless time from $t^* = 2$ to $t^* = 10$. Moreover, when the center deflection reaches steady state, it means the nanobeam has reached dynamic equilibrium, in which the electrostatic force between the two conducting electrodes are in balance with the elastic restoring force of nanobeam.

Table 3 shows the material and geometric properties of the clamped-clamped graphene nanobeam model in the following simulations. Figure 4 shows the variation of center deflection of the clamped-clamped graphene nanobeam model over time for applied voltage values ranging from 1 V to 2.05 V, for dimensionless time values from 0 to 100. The deflection increases nonlinearly with the increasing electrostatic force induced by the applied voltage. For voltage values ranging from 1 V to 2.04 V, the increasing deflection reaches a steady-state value. When a voltage of to 2.05 V, the graphene nanobeam collapses, at which point the movable electrode contacting with the stationary electrode. The relation between the dimensionless center deflection and applied voltage for a range of scale parameters is shown in Fig. 5, which makes evident the influence of nonlocal parameters on the pull-in voltage of the graphene nanobeam. Increasing the nonlocal parameters increases significantly the value of pull-in voltage, or delays the onset of the pull-in instability (which causes the beam collapse at higher pull-in voltage values) from $e_0a = 0$ *nm* to $e_0a = 2$ *nm*. The nonlocal effect containing the material parameter, internal and external characteristic length would decrease the maximum stable deflection at pull-in voltage of the nanostructure which is explained by the softening behavior [23]. In other word, the pull-in voltage with considering the nonlocal effect is larger than the pull-in voltage without considering the nonlocal effect. Note that the simulation results with $e_0a = 0$ *nm* yields numerical results consistent with classical elasticity results.

https://doi.org/10.1017/jmech.2018.41 Published online by Cambridge University Press

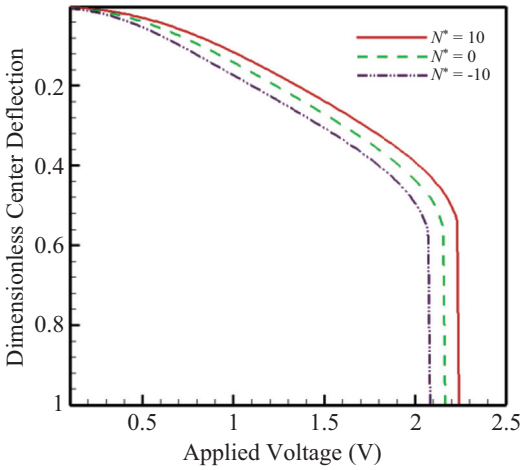


Fig. 6 Variation of dimensionless center deflection with applied voltage for different dimensionless residual stress (e_0a = 1 *nm*).

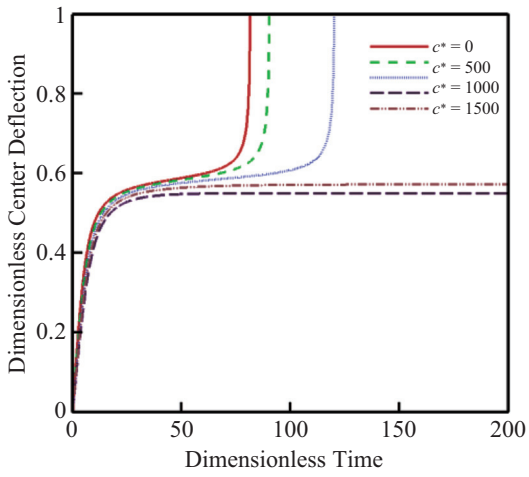


Fig. 7 Variation of dimensionless center deflection with dimensionless time for different dimensionless viscous damping (e_0a = 1 *nm*).

The effects of residual stress and viscous damping on the pull-in voltage for a graphene nanobeam were investigated, with e_0a fixed at 1 *nm*. The results are shown in Figs. 6 and 7, respectively. Figure 6 shows the variation of dimensionless center deflection with applied voltage for different values of dimensionless residual stress. In practice, the residual stress results from the manufacturing process for a graphene nanobeam, and can be tensile or compressive. Compared to the case without residual effects (N^* = 0), negative residual stress (N^* = -10) was seen to result in a lower pull-in voltage, and positive residual stress (N^* = 10) a higher pull-in voltage. This can be explained by the tensile residual stress (N^* = 10) stiffening the nanobeam and the compressive residual stress (N^* = -10) softening the nanobeam, respectively.

Figure 7 shows the variation of dimensionless center deflection as a function of the dimensionless time with different viscous damping values, and applied voltage 2.16 V. First, the figure reveals that the pull-in phenomenon occurs under the specified voltage without considering the viscous damping effect. For the case of c^* = 500 and c^* = 1000, the presence of dimensionless viscous damping was seen to delay the pull-in phenomenon (i.e. It causes the beam collapse at higher dimensionless time). Moreover, the results show that the graphene nanobeam reaches dynamic equilibrium with dimensionless viscous damping of c^* = 1500 and c^* = 2000. Since viscous damping produces a resistive force which opposes the electrostatic attraction, it is expected that its presence would reduce the deflection of the graphene nanobeam.

In the final part of the investigation, the role of geometric properties in determining the pull-in voltage of the nanobeam is examined. Figure 8 shows the relationship between the pull-in voltage and the length-gap ratio for several different nonlocal parameters. As the length-gap ratio increases, the pull-in voltage decreases. Perhaps more interestingly, the influence of scale parameters decreases as the length-gap ratio increases from 9 to 13, as can be seen from the fact that the results for e_0a =

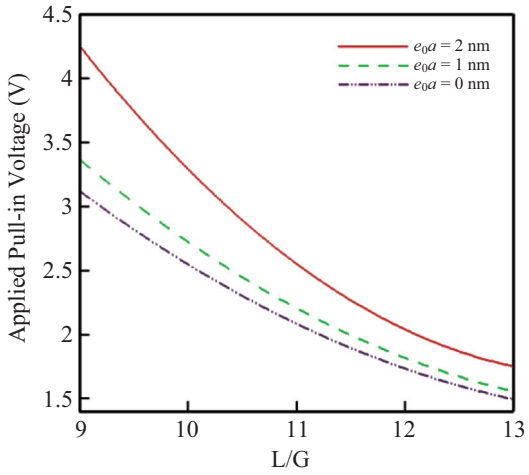


Fig. 8 Effect of the length-gap ratio on the pull-in voltage for different scale parameters.

1 *nm* and e_0a = 0 *nm* are similar, and that the pull-in voltage for a scale parameter of e_0a = 2 *nm* swiftly declines as the length-gap ratio increases. The effects of varying e_0a are consistent with previously discussed findings.

4. CONCLUSIONS

In this work, the HDTFDM is applied to the analysis of the nonlinear behavior of an nanobeam actuator whose model description is based on Eringen's nonlocal elasticity theory. The validity of the HDTFDM has been verified by comparing pull-in voltage results for a nanobeam with those obtained by using the LDL method as well previous numerical and experimental results, over a range of parameters. The HDTFDM results are in good agreement with previous literature. The nonlinear be-

https://doi.org/10.1017/jmech.2018.41 Published online by Cambridge University Press

havior of a clamped-clamped graphene nanobeam is then investigated, with detailed consideration of the effects of viscous damping, residual stresses, and length-gap ratio, modelled with the specification of nonlinear parameters. The results show that the tensile residual stress stiffens the nanobeam, increasing the pull-in voltage, whereas compressive residual stress has the opposite effect. The presence of viscous damping reduces the deflection of the nanobeam and delays the pull-in phenomenon. The pull-in voltage is also strongly dependent on the length-gap ratio, with a greater length-gap ratio exhibiting a lower pull-in voltage. The results of the present work also show that nonlocal effects play a significant role in determining the pull-in voltage of clamped-clamped graphene sheet nanobeam actuator.

ACKNOWLEDGEMENTS

This study acknowledges the support provided to this research by the Ministry of Science and Technology of Republic of China under Grant no. MOST104-2221-E006-009.

APPENDIX A

The Definition of Differential Transformation Theory

The differential transformation method [25-26] solves partial differential problems by transforming the governing equations into the form of algebraic equation. The advantage of differential methods over the integral method is its skill to transform nonlinear differential equations into polynomials by Taylor expansion. It is complicated to solve the nonlinear problems in the proceeding procedure by the integral method in comparison to the means of an iterative procedure by differential method. The basic definitions and principles of differential transformation method is given as follows:

Definition 1.

We assume $f(t)$ to be analytic function in a time domain D. The differential transformation of the function $f(t)$ is defined at time $t = t_0$, and the function $F(k,t_0)$ is defined in the C domain as

$$F(k,t_0) = M(k)\left[\frac{d^k}{dt^k}(q(t)f(t))\right]_{t=t_0}, \quad c \in C \tag{13}$$

where c belongs to non-negative integers and composes the C domain. $M(k)$ is the weighting factor and $q(t)$ is a kernel corresponding to $f(t)$, $M(k)$, and $q(t)$ that are both non-zero in D. The differential inverse transformation of $f(t)$ is expressed as

$$f(t) = \frac{1}{q(t)}\sum_{k=0}^{\infty}\frac{(t-t_0)^k}{k!}\frac{F(k,t_0)}{M(k)}, \quad \forall\ t \in D \tag{14}$$

Definition 2.

As explained in [26], set $M(k) = H^k/k!$ and $q(t)$, = 1 where H is the time interval, and $F(k)$ can be represented as

$$F(k) = T[f(t)] = \frac{H^k}{k!}\left[\frac{d^k f(t)}{dt^k}\right]_{t=0}, \quad c \in C \tag{15}$$

The inverse of differential transformation in Eq. (15) can be described as

$$f(t) = T^{-1}[F(k)] = \sum_{k=0}^{\infty}\left(\frac{t}{H}\right)^k F(k), \quad \forall\ t \in D \tag{16}$$

Substituting Eq. (15) into Eq. (16) becomes

$$f(t) = \sum_{k=0}^{\infty}\frac{t^k}{k!}\left[\frac{d^k f(t)}{dt^k}\right]_{t=0}, \quad \forall\ t \in D \tag{17}$$

The basic operators and some specific function of the differential transformation

https://doi.org/10.1017/jmech.2018.41 Published online by Cambridge University Press

(a) Linear operator

$$T\left[\varsigma u(t)+\xi v(t)\right]=\varsigma U(k)\ +\xi V(k) \tag{18}$$

(b) Convolution operator

i.

$$T\left[u(t)v(t)\right]=\sum_{l=0}^{k}U(l)V(k-l) \tag{19}$$

ii.

$$T\left[u^{p}(t)\right]=\sum_{l=1}^{k}\left[(p+1)l\right]U(l)U^{p}(k-l),\quad p\in N \tag{20}$$

(c) Differential operator

$$T\left[\frac{d^{r}u(t)}{dt^{r}}\right]=\frac{(k+r)!}{k!H^{r}}U(k+r),\quad \mathrm{r}\in \mathrm{N} \tag{21}$$

The differential transformation method is applied with respect to the time domain to each term in Eq. (12), i.e

$$T\left[\frac{\partial^{4}w^{*}}{\partial x^{*4}}\right]=\frac{\partial^{4}W(x^{*},k)}{\partial x^{*4}}$$

$$T\left[\frac{\partial w^{*}}{\partial t^{*}}\right]=\frac{(k+1)}{H}W\left(x^{*},k+1\right)$$

$$T\left[\frac{\partial^{2}w^{*}}{\partial t^{*2}}\right]=\frac{(k+1)(k+2)}{H^{2}}W\left(x^{*},k+2\right)$$

$$T\left[\int_{0}^{1}\left(\frac{\partial w^{*}}{\partial x^{*}}\right)^{2}dx^{*}\frac{\partial^{2}w^{*}}{\partial x^{*2}}\right]=\int_{0}^{1}\left(\frac{\partial W\left(x^{*},k\right)}{\partial x^{*}}\right)^{2}dx^{*}\frac{\partial^{2}W\left(x^{*},k\right)}{\partial x^{*2}}$$

$$T\left[\frac{\partial^{2}w^{*}}{\partial x^{*2}}\right]=\frac{\partial^{2}W\left(x^{*},k\right)}{\partial x^{*2}}$$

$$T\left[1\right]=\delta(k)$$

$$T\left[w^{*}\right]=W\left(x^{*},k\right)$$

$$T\left[w^{*2}\right]=\sum_{l=0}^{k}W\left(x^{*},l\right)W\left(x^{*},k-l\right)$$

$$T\left[w^{*3}\right]=\sum_{l=1}^{k}\left[(3+1)l-k\right]W\left(x^{*},l\right)W^{3}\left(x^{*},k-l\right)$$

$$T\left[w^{*4}\right]=\sum_{l=1}^{k}\left[(4+1)l-k\right]W\left(x^{*},l\right)W^{4}\left(x^{*},k-l\right)$$

$$T\left[w^{*5}\right]=\sum_{l=1}^{k}\left[(5+1)l-k\right]W\left(x^{*},l\right)W^{5}\left(x^{*},k-l\right) \tag{22}$$

where $\delta(k)=\begin{cases}1 & \text{for}\quad k=0\\ 0 & \text{otherwise}\end{cases}$, k and l are transform parameters.

After applying the finite difference method into the corresponding boundary and initial conditions, the governing

https://doi.org/10.1017/jmech.2018.41 Published online by Cambridge University Press

equation can be presented as

$$-\left(\frac{\alpha_0}{\Delta x^{*2}}\right)W_{i-1}(k+2)+\left(1+\frac{2\alpha_0}{\Delta x^{*2}}\right)W_i(k+2)-\left(\frac{\alpha_0}{\Delta x^{*2}}\right)W_{i+1}(k+2)=\frac{H^2}{(k+1)(k)}\times$$

$$\begin{Bmatrix}
-\dfrac{W_{i+2}(k)-4W_{i+1}(k)+6W_i(k)-4W_{i-1}(k)+W_{i-2}(k)}{\Delta x^{*4}}+N^*\dfrac{W_{i+1}(k)-2W_i(k)+W_{i-1}(k)}{\Delta x^{*2}} \\
-c^*\dfrac{(k+1)}{H}W_i(k+1)+\alpha_0 c^*\dfrac{(k+1)}{H}\dfrac{W_{i+1}(k+1)-2W_i(k+1)+W_{i-1}(k+1)}{\Delta x^{*2}} \\
-\alpha_0 N^*\dfrac{W_{i+2}(k)-4W_{i+1}(k)+6W_i(k)-4W_{i-1}(k)+W_{i-2}(k)}{\Delta x^{*4}} \\
+\alpha_4\int_0^1\left(\dfrac{W_{i+1}(k)-W_{i-1}(k)}{2\Delta x^*}\right)^2 dx^*\dfrac{W_{i+1}(k)-2W_i(k)+W_{i-1}(k)}{\Delta x^{*2}} \\
-\alpha_0\alpha_4\int_0^1\left(\dfrac{W_{i+1}(k)-W_{i-1}(k)}{2\Delta x^*}\right)^2 dx^*\dfrac{W_{i+2}(k)-4W_{i+1}(k)+6W_i(k)-4W_{i-1}(k)+W_{i-2}(k)}{\Delta x^{*4}} \\
+\alpha_1\begin{bmatrix}\delta(k)+2W_i(k)+3\sum_{l=0}^{k}W_i(l)W_i(k-l)\\ +4\sum_{l=1}^{k}[(3+1)l-k]W_i(l)W_i^3(k-l)\\ +5\sum_{l=1}^{k}[(4+1)l-k]W_i(l)W_i^4(k-l)\\ +6\sum_{l=1}^{k}[(5+1)l-k]W_i(l)W_i^5(k-l)\end{bmatrix}-6\alpha_0\alpha_1\begin{bmatrix}\delta(k)+4W_i(k)+10\sum_{l=0}^{k}W_i(l)W_i(k-l)\\ +20\sum_{l=1}^{k}[(3+1)l-k]W_i(l)W_i^3(k-l)\\ +35\sum_{l=1}^{k}[(4+1)l-k]W_i(l)W_i^4(k-l)\\ +56\sum_{l=1}^{k}[(5+1)l-k]W_i(l)W_i^5(k-l)\end{bmatrix} \\
+\alpha_1\alpha_2\begin{bmatrix}\delta(k)+W_i(k)+\sum_{l=0}^{k}W_i(l)W_i(k-l)\\ +\sum_{l=1}^{k}[(3+1)l-k]W_i(l)W_i^3(k-l)\\ +\sum_{l=1}^{k}[(4+1)l-k]W_i(l)W_i^4(k-l)\\ +\sum_{l=1}^{k}[(5+1)l-k]W_i(l)W_i^5(k-l)\end{bmatrix}-2\alpha_0\alpha_1\alpha_2\begin{bmatrix}\delta(k)+3W_i(k)+6\sum_{l=0}^{k}W_i(l)W_i(k-l)\\ +10\sum_{l=1}^{k}[(3+1)l-k]W_i(l)W_i^3(k-l)\\ +15\sum_{l=1}^{k}[(4+1)l-k]W_i(l)W_i^4(k-l)\\ +21\sum_{l=1}^{k}[(5+1)l-k]W_i(l)W_i^5(k-l)\end{bmatrix} \\
+\alpha_3\begin{bmatrix}\delta(k)+3W_i(k)+6\sum_{l=0}^{k}W_i(l)W_i(k-l)\\ +10\sum_{l=1}^{k}[(3+1)l-k]W_i(l)W_i^3(k-l)\\ +15\sum_{l=1}^{k}[(4+1)l-k]W_i(l)W_i^4(k-l)\\ +21\sum_{l=1}^{k}[(5+1)l-k]W_i(l)W_i^5(k-l)\end{bmatrix}-12\alpha_0\alpha_3\begin{bmatrix}\delta(k)+5W_i(k)+15\sum_{l=0}^{k}W_i(l)W_i(k-l)\\ +35\sum_{l=1}^{k}[(3+1)l-k]W_i(l)W_i^3(k-l)\\ +70\sum_{l=1}^{k}[(4+1)l-k]W_i(l)W_i^4(k-l)\\ +126\sum_{l=1}^{k}[(5+1)l-k]W_i(l)W_i^5(k-l)\end{bmatrix}
\end{Bmatrix} \tag{23}$$

The boundary condition also can be represented by first-order central difference method in Eq. (10)

$$W_i(k)=W_j(k)=0$$
$$\frac{W_{i+1}(k)-W_{i-1}(k)}{2\Delta x^*}=\frac{W_{j+1}(k)-W_{j-1}(k)}{2\Delta x^*}=0 \tag{24}$$

https://doi.org/10.1017/jmech.2018.41 Published online by Cambridge University Press

Where j is the final position of the beam in the x-direction. In a similar way, the initial condition in Eq. (11) can be rewritten as

$$W_i(0) = W_i(1) = 0 \tag{25}$$

In Eq. (21), W_{i-1}(k+2), W_i (k+2), W_{i+1}(k+2) are the unknown parameters and can be computed by using Thomas Matrix Algorithm (TDMA) with the corresponding boundary conditions and initial conditions.

REFERENCES

1. Lin, M. X. and Lai, H. Yi., "Analysis of Nonlocal Nonlinear Behavior of Graphene Sheet Circular Nanoplate Actuators Subject to Uniform Hydrostatic Pressure," *Microsystem Technologies*, **24**, pp. 919-928 (2018).
2. Park, S. and Horowitz, R., "Adaptive Control for the Conventional Mode of Operation of MEMS Gyroscopes," *Journal of Microelectromechanical Systems*, **12**, pp. 101-108 (2003).
3. Rutherglen, C., Jain, D. and Burke, P., "Nanotube Electronics for Radiofrequency Applications," *Nature Nanotechnology*, **4**, pp. 811-819 (2009).
4. Deotare, P. B., McCutcheon, M. W., Frank, I. W., Khan, M. and Lončar, M., "High Quality Factor Photonic Crystal Nanobeam Cavities," *Applied Physics Letters*, **94**, 121106 (2009).
5. Pei, J., Tian, F. and Thundat, T., "Glucose Biosensor Based on the Microcantilever," *Analytical Chemistry*, **76**, pp. 292-297 (2004).
6. Decca, R. S. *et al*., "Precise Comparison of Theory and New Experiment for the Casimir Force Leads to Stronger Constraints on Thermal Quantum Effects and Long-Range Interactions," *Annals of Physics*, **318**, pp. 37-80 (2005).
7. Sedighi, H. M., Daneshmand, F. and Zare, J., "The Influence of Dispersion Forces on the Dynamic Pull-in Behavior of Vibrating Nano-Cantilever Based NEMS Including Fringing Field Effect," *Archives of Civil and Mechanical Engineering*, **14**, pp. 766-775 (2014).
8. Soroush, R. *et al*., "Investigating the Effect of Casimir and Van Der Waals Attractions on the Electrostatic Pull-in Instability of Nano-Actuators," *Physica Scripta*, **82**, 045801 (2010).
9. Ramezani, A., Alasty, A. and Akbari, J., "Closed-Form Solutions of the Pull-in Instability in Nano-Cantilevers under Electrostatic and Intermolecular Surface Forces," *International Journal of Solids and Structures*, **44**, pp. 4925-4941 (2007).
10. Mousavi, T., Bornassi, S. and Haddadpour, H., "The Effect of Small Scale on the Pull-in Instability of Nano-Switches Using DQM," *International Journal of Solids and Structures*, **50**, pp. 1193-1202 (2013).
11. Dequesnes, M., Rotkin, S. V. and Aluru, N. R., "Calculation of Pull-in Voltages for Carbon-Nanotube-Based Nanoelectromechanical Switches," *Nanotechnology*, **13**, pp. 120-131 (2002).
12. Ramezani, A., Alasty, A. and Akbari, J., "Influence of Van Der Waals Force on the Pull-in Parameters of Cantilever Type Nanoscale Electrostatic Actuators," *Microsystem Technologies*, **12**, pp. 1153-1161 (2006).
13. Lin, W. H. and Zhao, Y. P., "Nonlinear Behavior for Nanoscale Electrostatic Actuators with Casimir Force," *Chaos, Solitons & Fractals*, **23**, pp. 1777-1785 (2005).
14. Pradhan, S. C. and Murmu, T., "Small Scale Effect on the Buckling of Single-Layered Graphene Sheets under Biaxial Compression *via* Nonlocal Continuum Mechanics," *Computational Materials Science*, **47**, pp. 268-274 (2009).
15. Murmu, T. and Pradhan, S. C., "Buckling Analysis of a Single-Walled Carbon Nanotube Embedded in an Elastic Medium Based on Nonlocal Elasticity and Timoshenko Beam Theory and Using DQM," *Physica E: Low-Dimensional Systems and Nanostructures*, **41**, pp. 1232-1239 (2009).
16. Eringen, A. C., "Nonlocal Polar Elastic Continua," *International Journal of Engineering Science*, **10**, pp. 1-16 (1972).
17. Eringen, A. C. and Edelen, D. G. B., "On Nonlocal Elasticity," *International Journal of Engineering Science*, **10**, pp. 233-248 (1972).
18. Eringen, A. C., "On Differential Equations of Nonlocal Elasticity and Solutions of Screw Dislocation and Surface Waves," *Journal of Applied Physics*, **54**, pp. 4703-4710 (2009).
19. Eringen, A. C., *Nonlocal Continuum Field Theories*, Springer Science & Business Media, 2002.
20. Murmu, T. and Pradhan, S. C., "Vibration Analysis of Nano-Single-Layered Graphene Sheets Embedded in Elastic Medium Based on Nonlocal Elasticity Theory," *Journal of Applied Physics*, **105**, 064319 (2009).
21. Yang, J., Jia, X. L. and Kitipornchai, S., "Pull-in Instability of Nano-Switches Using Nonlocal Elasticity Theory," *Journal of Physics D: Applied Physics*, **41**, 035103 (2008).
22. Reddy, J. N., "Nonlocal Nonlinear Formulations for Bending of Classical and Shear Deformation Theories of Beams and Plates," *International Journal of Engineering Science*, **48**, pp. 1507-1518 (2010).
23. Najar, F., El-Borgi, S., Reddy, J. N. and Mrabet, K., "Nonlinear Nonlocal Analysis of Electrostatic Nanoactuators," *Composite Structures*, **120**, pp. 117-128 (2015).
24. Zhou, J. K., "Differential Transformation and its Applications for Electrical Circuits," pp. 1279-1289 (1986).
25. Yu, L. T. and Chen, C. K., "The Solution of the Blasius Equation by the Differential Transformation Method," *Mathematical and Computer Modelling*,

https://doi.org/10.1017/jmech.2018.41 Published online by Cambridge University Press

28, pp. 101-111 (1998).

26. Chen, C. K., Lai, H. Y. and Liu, C. C., "Numerical Analysis of Entropy Generation in Mixed Convection Flow with Viscous Dissipation Effects in Vertical Channel," *International Communications in Heat and Mass Transfer*, **38**, pp. 285-290 (2011).
27. Chen, C. K., Lai, H. Y. and Liu, C. C., "Application of Hybrid Differential Transformation/Finite Difference Method to Nonlinear Analysis of Micro Fixed-Fixed Beam," *Microsystem Technologies*, **15**, pp. 813-820 (2009).
28. Shaat, M. and Mohamed, S. A., "Nonlinear- Electrostatic Analysis of Micro-Actuated Beams Based on Couple Stress and Surface Elasticity Theories," *International Journal of Mechanical Sciences*, **84**, pp. 208-217 (2014).
29. Hu, Y. C., Chang, C. M. and Huang, S. C., "Some Design Considerations on the Electrostatically Actuated Microstructures," *Sensors and Actuators A: Physical*, **112**, pp. 155-161 (2004).

(Manuscript received February 21, 2017,
accepted for publication July 19, 2018.)

https://doi.org/10.1017/jmech.2018.41 Published online by Cambridge University Press